Solid State Electrically Injected Exciton-Polariton Laser

Pallab Bhattacharya,* Bo Xiao, Ayan Das, Sishir Bhowmick, and Junseok Heo

Center for Photonic and Multiscale Nanomaterials, Department of Electrical Engineering and Computer Science, University of Michigan, Ann Arbor, Michigan 48109, USA

(Received 2 September 2012; revised manuscript received 21 January 2013; published 15 May 2013)

Inversionless ultralow threshold coherent emission, or polariton lasing, can be obtained by spontaneous radiative recombination from a degenerate polariton condensate with nonresonant excitation. Such excitation has, hitherto, been provided by an optical source. Coherent emission from a GaAs-based quantum well microcavity diode with electrical injection is observed here. This is achieved by a combination of modulation doping of the wells, to invoke polariton-electron scattering, and an applied magnetic field in the Faraday geometry to enhance the exciton-polariton saturation density. These measures help to overcome the relaxation bottleneck and to form a macroscopic and degenerate condensate as evidenced by angle-resolved luminescence, light-current characteristics, spatial coherence, and output polarization. The experiments were performed at 30 K with an applied field of 7 T.

DOI: 10.1103/PhysRevLett.110.206403 PACS numbers: 71.36.+c, 42.55.Sa, 78.45.+h, 85.35.Be

The strong coupling regime of emitter-photon interaction has been effectively exploited recently to demonstrate exciton-polariton lasers, which emit coherent light by spontaneous radiative recombination from a degenerate quantum state [1–9]. In these experiments the emitter, in the form of quantum wells (QWs) [3,4,9,10], quantum dots [11], or nanowire [12], is confined in an appropriate microcavity. While most of these systems have been optically pumped, polariton light emitting diodes with electrical injection have also been reported [13–15]. However, an electrically injected polariton laser has not been experimentally demonstrated.

Polariton relaxation can be enhanced by deploying polariton-electron scattering, which is more efficient in cooling the lower polaritons (LPs) compared to polariton-phonon scattering due to the small electron mass and a stronger charge-dipole interaction [16–18]. This additional scattering should facilitate the elimination, or reduction, of the relaxation bottleneck. In an optically excited system, it has been demonstrated that photoexcitation of a secondary quantum well produces a two-dimensional electron gas, which is transferred to the primary quantum well and interacts with LPs contained therein [17]. In an electrically injected microcavity device, modulation doping with electrons can be achieved more easily by introducing a sheet of Si dopants in the barrier regions at a suitable distance from the quantum wells. However, even with an enhancement of the scattering rate, the system may transition to the weak coupling regime before polariton lasing can be observed. It is known that in semiconductors a magnetic field shrinks the exciton wave function and Bohr radius and enhances the electron-hole overlap, resulting in an increase in oscillator strength f. In a system with strong coupling, since $\Omega \propto \sqrt{f}$, the Rabi splitting also increases with field. This behavior has been demonstrated in magneto-photoluminescence and magneto-absorption measurements [19–21]. The reduction in the exciton Bohr radius (to $\sim$6 nm for an applied field of 7 Tesla) helps to increase the exciton-polariton saturation density. Therefore, in the presence of a magnetic field and polariton electron scattering, it should be possible to observe coherent emission in the appropriate temperature range. In this work we have investigated strong coupling effects in a quantum well microcavity diode with modulation doping of the wells in the presence of an applied magnetic field of 7 T at $T = 30$ K. Polariton lasing from the microcavity diode is observed under these conditions. A second threshold, corresponding to photon lasing with population inversion, is also observed from the same diode at a current density $\sim$3 orders of magnitude higher than the polariton lasing threshold.

The *p-i-n* multiquantum-well microcavity diode used in our experiment is described in the Supplemental Material [22]. The current densities quoted in the following are based on a uniform injection across the mesa diameter. To introduce electrons into the $In_{0.1}Ga_{0.9}As/GaAs$ QWs, a 1 nm thick layer at a distance of 10 nm above each pair of QWs was Si(n)-doped with a concentration of $n = 1 \times 10^{17}$ cm^{-3}. This corresponds to a thermally ionized electron sheet density of $n_s = 1 \times 10^{10}$ cm^{-2} in the QWs. Since the modulation doping is highly degenerate, the impurity band overlaps with the conduction band, and hence the dopants require no energy for ionization. The quality factor (Q) of the cavity is estimated to be 6052 based on a low temperature (20 K) microphotoluminescence measurement of the cavity mode at 1.3744 eV with a linewidth $\gamma_C = 0.23$ meV, corresponding to a cavity mode lifetime of $\tau_C = 3$ ps. The experimental value of the Q factor of the cavity is limited by nonideality of the grown QWs and the numerical aperture of the objective lens which collects emission from zero and nonzero in-plane wave vectors within the collection angle. The cavity Q is

estimated to be ~12 000 from finite-difference time-domain calculations.

Figure 1(a) shows the electroluminescence (EL) spectra at 30 K as a function of detection angle measured in the absence of applied magnetic field. Similar spectra can also be obtained from angle-resolved photocurrent measurement [15,21]. A weaker peak at the higher energy side of the LP peak is also observed and can be identified as the middle polariton (MP) due to the coupling between the cavity photons and trions in the presence of the 2D electron gas introduced by modulation doping. It is therefore not accurate to characterize the strength of strong coupling by simply quoting the value of Rabi splitting between the upper polariton (UP) and LP. Instead, the interactions can be more appropriately described by two coupling parameters. The coupling strengths for exciton-photon ($\Omega_{HH} = 5.1$ meV) and trion-photon ($\Omega_{X^-} = 1.8$ meV) interactions and the detuning ($\delta = E_{cav} - E_X = -3.5$ meV) were extracted by fitting the polariton emission spectra with a 3×3 coupled harmonic oscillator model (shown as solid lines on the dispersion curves), in which we have used an exciton energy of 1.3779 eV with a linewidth of 1.3 meV measured at $T = 30$ K, a trion energy of 1.376 eV with a linewidth of 1.5 meV and a cavity photon linewidth of 0.23 meV. We then measured angle-resolved EL from the device in the presence of a magnetic field of 7 T (the highest field attainable in our system) parallel to the growth axis (Faraday geometry) with $J = 2$ A/cm^2. In Fig. 1(b), it can be seen from the angle-resolved spectra that the exciton energy has increased to 1.3803 eV as a result of the diamagnetic shift caused by the magnetic field. The dispersion curves obtained by fitting the resonances in the spectra at $B = 7$ T reveal that Ω_{HH} has increased from 5.1 to 6.98 meV. However, Ω_{X^-} remains almost unchanged. At the same time, the system becomes more negatively detuned ($\delta = -5.9$ meV). The increase of heavy-hole exciton-photon coupling strength allows strong coupling to persist up to higher injection currents.

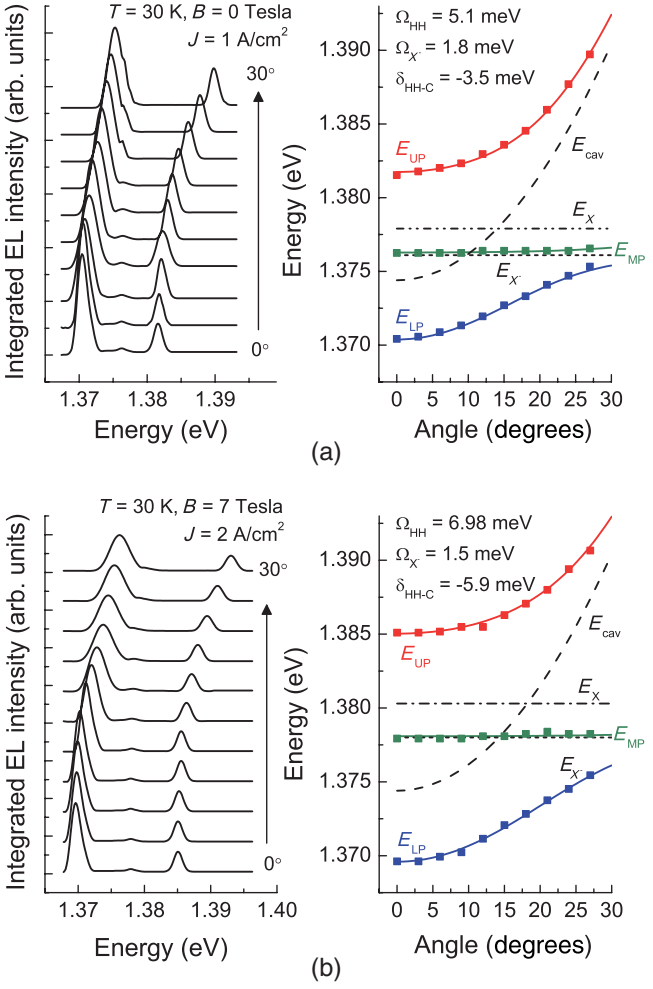

FIG. 1 (color online). Measured angle-resolved electroluminescence spectra and the corresponding dispersion characteristics obtained from the solutions to a 3×3 coupled harmonic Hamiltonian (a) at $B = 0$ T for a current density of 1 A/cm^2 in the continuous mode and (b) at $B = 7$ for a current density of 2 A/cm^2. The spectra reveal anticrossing between a LP branch (blue), a weak MP branch (green) originating from the trion (X^-)-photon interaction and a UP branch (red). The heavy-hole exciton-photon coupling parameter (Ω_{HH}) increases from 5.1 to 6.98 meV in the presence of the magnetic field.

Electroluminescence from the device as a function of continuous wave (cw) injection current density was then measured in the normal direction under $B = 7$ T. In Fig. 2(a), a clear nonlinear threshold is observed at a current density of ~12 A/cm^2, accompanied by a reduction of LP emission linewidth. The superlinear increase of emission intensity as a function of injection current below threshold can be attributed to enchanced polariton relaxation to the ground state, which was also observed in other electrically injected polariton devices [13]. It is of interest to note that Solynshkov *et al.* [23] have predicted a threshold current density of 50 A/cm^2 in an electrically injected GaN microcavity polariton laser at room temperature. The LP coherence time of 6.1 ps, corresponding to the minimum linewidth of 0.68 meV at threshold, is larger than the LP radiative lifetime $\tau_{LP} \sim \tau_C/|C|^2 =$ 4.2 ps. As the current density increases above threshold, the LP emission linewidth increases again due to the exciton-exciton interaction. We have calculated the LP density from the injection current density by using the relation $n_{LP} = J\tau_{total}/q$, where J is the current density and τ_{total} is the total lifetime of excitons. The latter was determined to be 763 ps from time-resolved photoluminescence measurements performed on the device (see Supplemental Material [22]). The polariton density at the nonlinear threshold is found to be 5.9×10^{10} cm^{-2}. As can be seen in Figs. 2(b) and 2(c), with further increase in injection current, the transition from strong to weak coupling takes place and at $J = 70$ A/cm^2

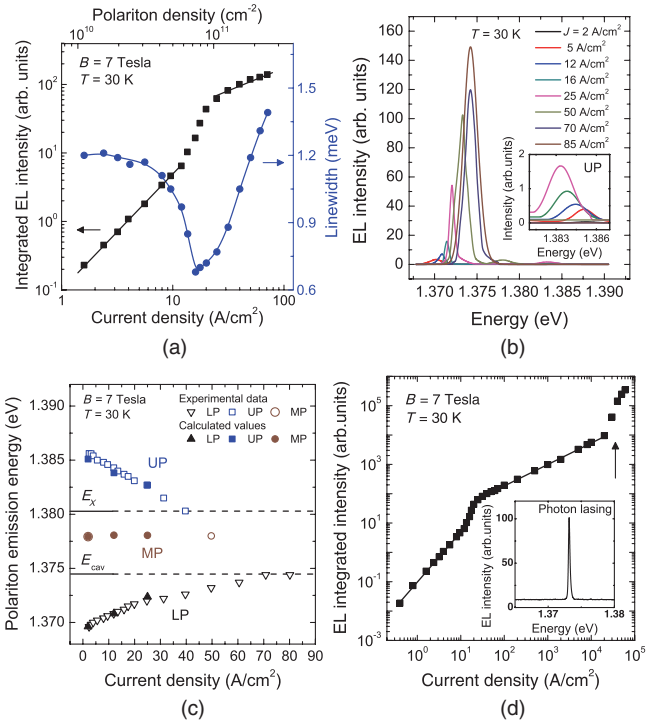

FIG. 2 (color online). Polariton lasing characteristics. (a) Integrated EL intensity and LP emission linewidth at $B = 7$ T measured as a function of injected current density. The nonlinear threshold for polariton lasing is at $J = 12$ A/cm^2 and the emission linewidth decreases from 1.2 to 0.68 meV. (b) EL spectra measured at different injection densities at normal detection angle. The inset shows the magnified UP region. (c) LP and UP peak energies as a function of injection current density reveal a transition to the weak coupling regime at $J = 70$ A/cm^2. The peak observed at $J = 50$ A/cm^2 is likely due to MP emission. (d) Two-threshold behavior showing the polariton and photon lasing thresholds. The photon lasing spectrum at $J = 4 \times 10^4$ A/cm^2 is shown as an inset.

(corresponding to a density of 3.4×10^{11} cm^{-2}) the LP emission coincides with the cavity mode. The coupling strength between HH excitons and photons decreases with increasing current density due to the reduced QW exciton oscillator strength caused by the phase-space filling effect when more carriers are injected. With further increase in current injection (pulsed beyond $J = 85$ A/cm^2 with 5% duty cycle to avoid device heating), photon lasing is observed with a threshold $J = 2 \times 10^4$ A/cm^2, a value that is $\sim 3 \times 10^3$ times the polariton lasing threshold. The two-threshold behavior is shown in Fig. 2(d) at $B = 7$ T with the photon lasing spectrum at $J = 4 \times 10^4$ A/cm^2 as an inset. The calculated injected power density at the photon lasing threshold is 40 kW/cm^2 which is comparable to values quoted for similar sized vertical cavity surface emitting lasers [24]. It is important to note that in the present case the device is maintained at 30 K. Nonetheless, the device temperature is most certainly higher than 30 K. It is evident that the combined effects of modulation doping and magnetic field contribute to polariton lasing. On the same device, we have measured the total integrated EL intensity as a function of injection current density in the absence of magnetic field at 30 K [25]. The system entered the weak coupling regime before the onset of the nonlinear threshold, which confirms that the saturation density was reached before polariton lasing could take place.

In Figs. 3(a)–3(d), we show the polariton emission intensity in momentum space for different injection current densities as false color plots, obtained from angle-resolved EL measurements at $B = 7$ T. The plots reveal that below the polariton lasing threshold current density, the LP emission has a broad distribution in both energy and momentum, whereas above threshold, the emission originates from a condensate formed at $k_{\|} \sim 0$ with a linewidth of 0.8 meV and $\Delta k \sim 4.3 \times 10^3$ cm^{-1} (note that the experimental angular resolution is 1° which corresponds to a $\Delta k \sim 1.2 \times 10^3$ cm^{-1}). At $J = 80$ A/cm^2 [Fig. 3(d)], the emission spectrum in the weak coupling regime corresponds to that of the cavity mode, as expected. We have calculated the LP occupancy in $k_{\|}$-space from these plots [26], and these are shown in Fig. 3(d). There is no obvious relaxation bottleneck at all injection current densities. Below and up to the polariton lasing threshold, the distribution of LPs can be analyzed by a Maxwell-Boltzmann distribution, which suggests that electron-polariton scattering effectively thermalizes the LP distribution [16]. At threshold for $J = 12$ A/cm^2, the occupancy can be analyzed by a Maxwell-Boltzmann distribution with $T_{\mathrm{LP}} = 57$ K. Above threshold, the emission becomes sharply peaked at small angles, showing condensation in k space. Both the nonlinearity at the polariton lasing threshold and the large population in the low energy states directly result from the stimulated scattering of polaritons towards the ground state, which is essential for polariton lasing [5].

The long-range spatial coherence properties of the polariton emission were measured with a Mach-Zehnder interferometer described in the Supplemental Material [22]. The presence of finite-sized condensates in a 2D microcavity has been predicted by theoretical calculations [27,28] and has been experimentally observed in a CdTe system [3]. The interference measurement gives an estimate of the spatial coherence length of the polariton condensate. Figure 4(a) shows the first-order degree of coherence $|g_1|$ as a function of position shift (or the amount of overlap) between the two copies of images obtained from the interference patterns [29]. At threshold, with $J = 12$ A/cm^2 the degree of coherence increases to 15%, whereas above threshold, at $J = 25$ A/cm^2, a maximum value of 25% is observed for complete overlap between the two images. The width of the first-order degree of coherence [Fig. 4(a)] is ~ 15 μm, indicating the approximate size of the condensation droplets formed above threshold. Finally, the polarization of the LP

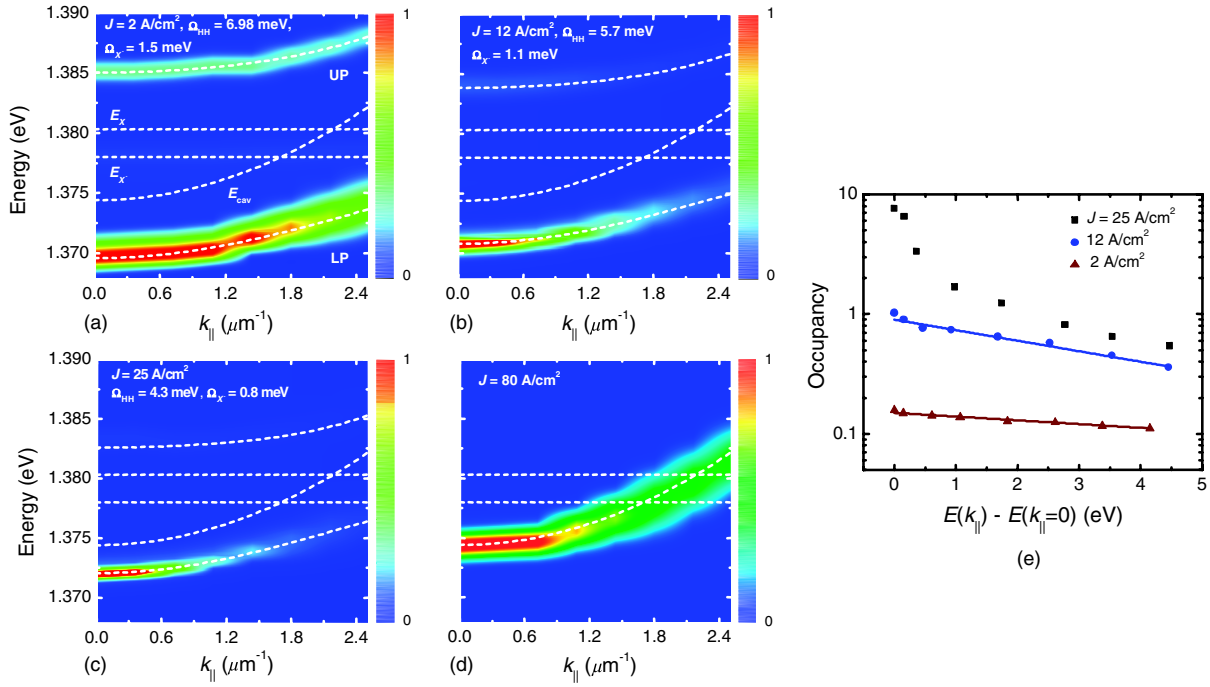

FIG. 3 (color online). Momentum distribution of polaritons at different injection current densities (a) $J = 2$ A/cm^2, (b) $J = 12$ A/cm^2, (c) $J = 25$ A/cm^2, and (d) $J = 80$ A/cm^2 obtained from angle-resolved measurements and displayed as false color plots. (e) Occupancy per LP state as a function of the energy difference $E(k_\parallel) - E(k_\parallel = 0)$ obtained from angle-resolved EL spectra at different injection densities. We have arbitrarily set the ground state occupancy equal to unity at threshold. The solid curves indicate fits obtained with Maxwell-Boltzmann distributions (see text).

emission was measured as a function of the injected current density [Fig. 4(b)]. The emission was found to be almost depolarized below threshold (12 A/cm^2) and elliptically polarized above threshold with the degree of linear polarization ρ_{lin} increasing to 0.51 and the circular polarization ρ_{cir} to 0.41 from noise limited values. The linear polarization is along a [110] crystallographic axis [3,4,10]. The circular polarization originates from the Zeeman splitting induced by the magnetic field and subsequent LP condensation in the σ^+-state [30,31].

In conclusion, we observe coherent emission from a GaAs-based modulation-doped quantum well-microcavity diode in the strong coupling regime with the application of an external magnetic field. The combined effects of modulation doping and magnetic field contribute to polariton lasing.

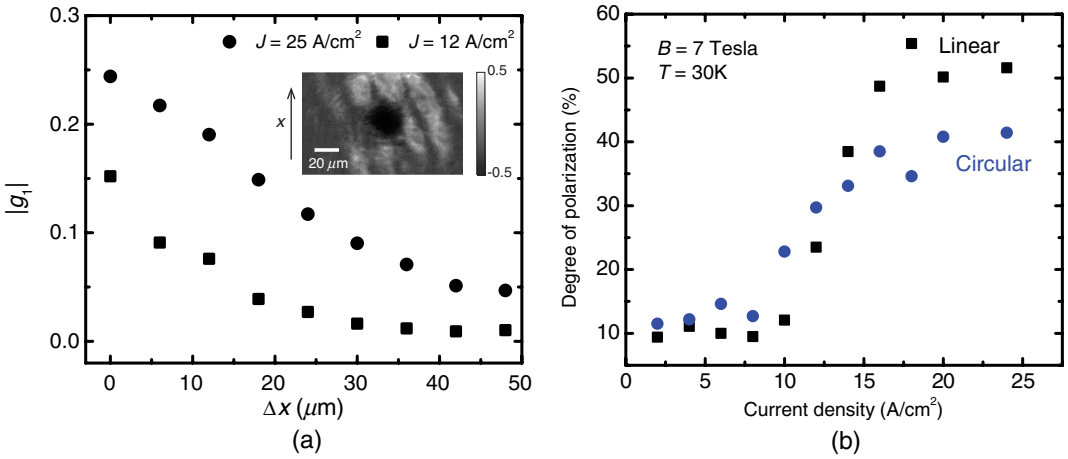

FIG. 4 (color online). First-order spatial coherence and degree of polarization of light output. (a) Amplitude of the first-order degree of coherence measured as a function of the displacement between a double image of the polariton condensate for two injected current densities. The inset shows the corresponding interference pattern for complete overlap of the two images. (b) Degree of linear ρ_{lin} and circular ρ_{cir} polarization measured as a function of injected current density.

This work is supported by the National Science Foundation under the MRSEC Program (Grant DMR 1120923) and Grant ECS 1220715.

*pkb@umich.edu

[1] C. Weisbuch, M. Nishioka, A. Ishikawa, and Y. Arakawa, Phys. Rev. Lett. **69**, 3314 (1992).
[2] G. Khitrova, H. M. Gibbs, F. Jahnke, M. Kira, and S. W. Koch, Rev. Mod. Phys. **71**, 1591 (1999).
[3] J. Kasprzak *et al.*, Nature (London) **443**, 409 (2006).
[4] R. Balili, V. Hartwell, D. Snoke, L. Pfeiffer, and K. West, Science **316**, 1007 (2007).
[5] A. Imamoglu, R. J. Ram, S. Pau, and Y. Yamamoto, Phys. Rev. A **53**, 4250 (1996).
[6] H. Deng, G. Weihs, D. Snoke, J. Bloch, and Y. Yamamoto, Proc. Natl. Acad. Sci. U.S.A. **100**, 15 318 (2003).
[7] S. Christopoulos *et al.*, Phys. Rev. Lett. **98**, 126405 (2007).
[8] S. Kéna-Cohen and S. R. Forrest, Nat. Photonics **4**, 371 (2010).
[9] D. Bajoni, P. Senellart, E. Wertz, I. Sagnes, A. Miard, A. Lemaître, and J. Bloch, Phys. Rev. Lett. **100**, 047401 (2008).
[10] G. Christmann, R. Butté, E. Feltin, J. Carlin, and N. Grandjean, Appl. Phys. Lett. **93**, 051102 (2008).
[11] M. Nomura, N. Kumagai, S. Iwamoto, Y. Ota, and Y. Arakawa, Nat. Phys. **6**, 279 (2010).
[12] A. Das, J. Heo, M. Jankowski, W. Guo, L. Zhang, H. Deng, and P. Bhattacharya, Phys. Rev. Lett. **107**, 066405 (2011); A. Das, J. Heo, A. Bayraktaroglu, W. Guo, T.-K. Ng, J. Phillips, B. S. Ooi, and P. Bhattacharya, Opt. Express **20**, 11 830 (2012).
[13] S. I. Tsintzos, N. T. Pelekanos, G. Konstantinidis, Z. Hatzopoulos, and P. G. Savvidis, Nature (London) **453**, 372 (2008).
[14] A. A. Khalifa, A. P. D. Love, D. N. Krizhanovskii, M. S. Skolnick, and J. S. Roberts, Appl. Phys. Lett. **92**, 061107 (2008).
[15] D. Bajoni, E. Semenova, A. Lemaître, S. Bouchoule, E. Wertz, P. Senellart, and J. Bloch, Phys. Rev. B **77**, 113303 (2008).
[16] G. Malpuech, A. Kavokin, A. Di Carlo, and J. J. Baumberg, Phys. Rev. B **65**, 153310 (2002).
[17] P. G. Lagoudakis, M. Martin, J. Baumberg, A. Qarry, E. Cohen, and L. Pfeiffer, Phys. Rev. Lett. **90**, 206401 (2003).
[18] M. Perrin, J. Bloch, A. Lemaitre, and P. Senellart, Phys. Status Solidi C **2**, 759 (2005).
[19] T. A. Fisher, A. M. Afshar, M. S. Skolnick, D. M. Whittaker, and J. S. Roberts, Phys. Rev. B **53**, R10469 (1996).
[20] J. Tignon, R. Ferreira, J. Wainstain, C. Delalande, P. Voisin, M. Voos, R. Houdré, U. Oesterle, and R. Stanley, Phys. Rev. B **56**, 4068 (1997).
[21] P. Bhattacharya, A. Das, S. Bhowmick, M. Jankowski, and C. Lee, Appl. Phys. Lett. **100**, 171106 (2012).
[22] See Supplemental Material at http://link.aps.org/supplemental/10.1103/PhysRevLett.110.206403 for a description of the device structure, its near-field image, TRPL results of QW excitons and a description of the interference measurement.
[23] D. Solnyshkov, E. Petrolati, A. Di Carlo, and G. Malpuech, Appl. Phys. Lett. **94**, 011110 (2009).
[24] J. Geske, M. MacDougal, G. Cole, and D. Snyder, Proc. SPIE Int. Soc. Opt. Eng. **6287**, 628703 (2006).
[25] A. Das, B. Xiao, S. Bhowmick, and P. Bhattacharya, Appl. Phys. Lett. **101**, 131112 (2012).
[26] The polariton occupation number per $k_\parallel$ state by using the formula, $I_{\mathrm{LP}}(k_\parallel) = \eta N_{\mathrm{LP}}(k_\parallel)|C(k_\parallel)|^2 M/\tau_C$, where η is the collection efficiency, $\tau_C/|C(k_\parallel)|^2$ is the radiative lifetime of the LPs, M is the number of transverse states included in the detection cone and $|C(k_\parallel)|^2$ is the photon fraction at a wave-vector $k_\parallel$. The number of states within the detection cone is given by $M = D^2/16(k_0\Delta\theta)^2$, where D is the diameter of the emission spot, $k_0 = 2\pi/\lambda$ and $\Delta\theta$ is the detection half angle. τ_C is estimated from the cavity Q, and the value of η is estimated by replacing the sample with a source of known power (a laser with suitable attenuation).
[27] G. Malpuech, Y. G. Rubo, F. P. Laussy, P. Bigenwald, and A. V. Kavokin, Semicond. Sci. Technol. **18**, S395 (2003).
[28] D. Sarchi and V. Savona, Phys. Rev. B **75**, 115326 (2007).
[29] A. A. High, J. R. Leonard, A. T. Hammack, M. M. Fogler, L. V. Butov, A. V. Kavokin, K. L. Campman, and A. C. Gossard, Nature (London) **483**, 584 (2012).
[30] A. V. Larionov, V. D. Kulakovskii, S. Höfling, C. Schneider, L. Worschech, and A. Forchel, Phys. Rev. Lett. **105**, 256401 (2010).
[31] V. D. Kulakovskii, A. S. Brichkin, S. V. Novikov, C. Schneider, S. Höfling, M. Kamp, A. Forchel, and N. A. Gippius, Phys. Rev. B **85**, 155322 (2012).